Atmospheric
Chemistry
and Physics

Open Access

# Major contribution of neutral clusters to new particle formation at the interface between the boundary layer and the free troposphere

C. Rose[1], K. Sellegri[1], E. Asmi[2], M. Hervo[1], E. Freney[1], A. Colomb[1], H. Junninen[3], J. Duplissy[3], M. Sipilä[3], J. Kontkanen[3], K. Lehtipalo[3,4], and M. Kulmala[3]

[1]Laboratoire de Météorologie Physique CNRS UMR6016, Observatoire de Physique du Globe de Clermont-Ferrand, Université Blaise Pascal, Clermont-Ferrand, France
[2]Finnish Meteorological Institute, P.O. Box 503, 00101 Helsinki, Finland
[3]Department of Physics, University of Helsinki, Helsinki, Finland
[4]Airmodus Ltd, Gutaf Hällströmin katu 2, 00560 Helsinki, Finland

*Correspondence to:* K. Sellegri (k.sellegri@opgc.univ-bpclermont.fr)

**Abstract.** The formation of new aerosol particles in the atmosphere is a key process influencing the aerosol number concentration as well as the climate, in particular at high altitude, where the newly formed particles directly influence cloud formation. However, free tropospheric new particle formation (NPF) is poorly documented due to logistic limitations and complex atmospheric dynamics around high-altitude stations that make the observation of this day-time process challenging. Recent improvements in measurement techniques make now possible the detection of neutral clusters down to $\sim 1$ nm sizes, which opens new horizons in our understanding of the nucleation process. Indeed, only the charged fraction of clusters has been reported in the upper troposphere up to now. Here we report day-time concentrations of charged and neutral clusters (1 to 2.5 nm mobility diameter) recorded at the interface between the boundary layer (BL) and the FT as well as in the FT at the altitude site of Puy de Dôme (1465 m a.s.l.), central France, between 10 and 29 February 2012. Our findings demonstrate that in the FT, and especially at the interface between the BL and the FT, the formation of 1.5 nm neutral clusters significantly exceeds the one of ionic clusters during NPF events, clearly indicating that they dominate in the nucleation process. We also observe that the total cluster concentration significantly increases during NPF events compared to the other days, which was not clearly observed for the charged cluster population in the past. During the studied period, the nucleation process does not seem to be sulfuric acid-limited and could be promoted by the transport of pollutants to the upper troposphere, coupled with low temperatures.

## 1 Introduction

New particle formation directly impacts the total atmospheric aerosol particle concentration and has an indirect effect on climate through cloud-related radiative processes (Makkonen et al., 2012). The formation of aerosol particles has been observed and studied in various environments around the world. It appears that depending on the location, new particle formation (NPF) events do have specificities in term of intensity and space scales, both horizontal (Kulmala et al., 2004) and vertical (Boulon et al., 2011). The formation of new particles in the FT is particularly important as actual global models predict that it contributes to an important fraction of the total atmospheric column aerosol number concentration (Merikanto et al., 2009) and hence potential CCN number concentrations (Spracklen et al., 2008). However, observation of NPF at high altitude is still scarce, especially using the instrumentation adapted to the study of nanometer-sized clusters.

Aerosol formation results from a complex sequence of different processes including the production of clusters from gaseous precursors and the growth of these clusters to particles. Despite the fact that instrumentation is continuously improved, our understanding of the aerosol formation mech-

anism is still limited. Especially challenging tasks are to quantitatively detect neutral clusters and identify the chemical species involved in the first step of the NPF.

Until a few years ago, the measurement techniques able to detect the smallest cluster sizes were based on electrostatic methods, such as the NAIS (Neutral Air Ion Spectrometer; Mirme and Mirme, 2013). These methods require artificial charging of neutral particles prior to the measurement. Studies concerning the NAIS sampling technique showed that reliable measurements of neutral cluster concentrations could not be ensured for diameters smaller than ∼ 2 nm because of the post-filtering process of corona-generated ions (Asmi et al., 2009; Manninen et al., 2011). Recent improvements of condensation techniques make it now possible to measure the concentrations and the size distributions of charged as well as neutral particles down to ∼ 1 nm sizes (Kim et al., 2003; Vanhanen et al., 2011; Kuang et al., 2012a). This size limit appears to be more relevant for the study of nucleation compared to the 2 nm size limit of the NAIS since it was recently shown that atmospheric nucleation occurs at a size 1.5 nm ± 0.4 nm (Kulmala et al., 2007; Kirkby et al., 2011; Kulmala et al., 2013). Using PSM (particle size magnifier, Vanhanen et al., 2011) measurements, Kulmala et al. (2013) have recently reported a high variability, both in term of spatial and temporal scales, of neutral cluster concentrations at boundary layer sites. In Hyytiälä, Finland, they were also able to quantify the fraction of particles produced exclusively by the neutral pathway, i.e. excluding ion-mediated nucleation and recombination of oppositely charged ions (Kontkanen et al., 2013). Several studies performed prior to the development of the PSM have reported that the charged nucleation pathway seemed to be a more favourable route at high altitude compared to boundary layer (BL) stations for the formation of new particles (Boulon et al., 2010; Manninen et al., 2010).

In this paper, we report the diurnal variability of total, charged and neutral cluster concentrations as well as NPF event characteristics measured between 10 and 29 February 2012 using PSM and NAIS data recorded in clear sky conditions at the Puy de Dôme station (7 days available). This period was selected due to the occurrence of very low temperatures in central and western Europe, which led to unusually low BL height coupled with increased pollution levels. The low BL height permitted the Puy de Dôme station to be in the free troposphere (FT) even during day-time, when nucleation occurred, or, more frequently, at the interface between the BL and the FT. Thus, the main purpose of this paper is to investigate cluster formation and concentrations in these unusual conditions, with a special focus on neutral clusters.

## 2 Measurements and methods

### 2.1 Measurement site

Measurements were carried out at the Puy de Dôme (PUY) site (45°46′ N, 2°46′ E) in central France (part of European networks EMEP/GAW/ACTRIS). The station is located at the top of the Puy de Dôme mountain (1465 m a.s.l) and is mainly surrounded by fields and forest. The nearest town, Clermont-Ferrand (300 000 inhabitants), is located 16 km east of the mountain at 396 m a.s.l. A more detailed description of the station can be found in Freney et al. (2011).

### 2.2 Instrumentation

#### 2.2.1 The neutral cluster and air ion spectrometer (NAIS)

The charged cluster size distributions were recorded with a NAIS (Airel Ltd., Mirme et al., 2007; Mirme and Mirme, 2013) which ensures ion measurement in the mobility range 0.0013–3.2 cm$^2$ V$^{-1}$ s$^{-1}$, corresponding to particle Millikan diameters between 0.8 and 42 nm. The instrument was operating on the roof of the station behind an individual non-heated short inlet (30 cm). This setup implies that measurements are directly influenced by cloudy conditions. The AIS sampling method is based on the simultaneous measurement of positively and negatively charged particles with two identical cylindrical Differential Mobility Analysers (DMA). Each analyser uses a sample flow rate of 30 L min$^{-1}$ and a sheath flow rate of 60 L min$^{-1}$, which minimizes diffusion losses and ensures significant signal to noise ratio, even in the case of low concentrations. The inner cylinder of each DMA is divided into four isolated rings charged with a constant voltage during a measurement cycle. The outer cylinder is made of 21 isolated rings connected to 21 electrometers. Naturally charged aerosol particles are moved in the DMA by a radial electric field from the inner cylinder to the outer one. The current carried by ions entering the DMA is amplified and measured with electrometers. After a measurement cycle, the instrument runs an offset measurement in order to estimate the noise of the electrometers. During the offset measurement, all the particles, both neutral and charged, must be removed from the sample air before they enter the DMAs. For that purpose, all the particles are thus charged with a unipolar corona charger and electrically filtered before reaching the DMAs.

The NAIS also allows the detection of total particles after a pre-charging process during which particles are charged by ions originating from a corona discharge. The sampling analysis method is then similar to the one described for the ions.

## 2.2.2 The particle size magnifier (PSM)

The total (neutral + ion) cluster concentrations ($N_{tot}$) were measured with a PSM (Airmodus A09, Vanhanen et al., 2011) which allows cluster detection down to $\sim 1$ nm sizes. The PSM is a mixing type instrument in which the activation of particles is based on a rapid and turbulent mixing of aerosol and heated air saturated with diethylene glycol (DEG). Optical particle counting is done with an ordinary CPC (TSI 3010). The sample flow rate of the PSM is fixed at 2.5 L min$^{-1}$ while the saturator flow rate can be varied in the range 0.1–1 L min$^{-1}$, which corresponds to varying the 50 % activation diameter of the instrument between 1 and 2.5 nm by changing the mixing ratio of the DEG vapour. For the measurements used in this study, the PSM was operating in a scanning mode with 120 steps between saturator flow rates 0.1–1 L min$^{-1}$ and a time resolution of 4 min.

## 2.2.3 Atmospheric pressure interface time of flight mass spectrometer (APi-TOF)

In this study, APi-TOF measurements (Junninen et al., 2010) were not directly used to investigate the cluster composition but rather to modify a proxy for sulfuric acid concentrations at the PUY, as explained in Sect. 2.3.1. The method used to calculate neutral H$_2$SO$_4$ concentrations from naturally charged negative ion measurements conducted with the APi-TOF is similar to the one proposed by Eisele (1989). We obtained a calibration coefficient specific to the APi-TOF from the ratio of the sulfuric acid concentration calculated from the APi-TOF naturally charged ion signals to sulfuric acid concentration measured by a calibrated CI-APi-TOF (Jokinen et al., 2012). The comparison was achieved during a field campaign that took place in Hyytiälä atmospheric station (Hari and Kulmala, 2005).

## 2.2.4 LIDAR measurements

In order to get an estimation of the BL height, here assumed to be equal to the aerosol mixing layer height, LIDAR measurements were achieved from the roof of the Laboratoire de Météorologie Physique (45°45′ N, 3°6′ E, 410 m a.s.l.). The LIDAR is a Raymetrics Rayleigh–Mie LIDAR emitting at 355 nm, with both parallel and orthogonal polarization channels. The spatial resolution of the LIDAR is 7.5 m. The instrument provides volume backscatter and extinction profiles, as well as the depolarization ratio and water vapour mixing ratio. A more complete description of the LIDAR is available in Hervo et al. (2012). The method used for the determination of the BL height is detailed in Sect. 2.3.2.

## 2.2.5 Auxiliary measurements

Auxiliary measurements were used to explain the observed NPF and cluster concentration features reported in the present study. Numerous atmospheric parameters such as global radiation, wind speed and direction, temperature, pressure and relative humidity (RH) as well as atmospheric trace gases (including SO$_2$, CO and NO$_2$) and particulate black carbon (BC) are continuously recorded at the station. SO$_2$ measurements were performed using a low-level SO$_2$ analyser (pulsed fluorescence TEI 43CTL) while BC measurements were achieved with a Multi Angle Absorption Photometer (MAAP 5012, central wavelength at 637 nm). The aerosol particle number size distributions were measured with a custom-built Scanning Mobility Particle Sizer (SMPS) operating in the size range 10–420 nm. The SMPS, as well as the PSM, were operating behind a Whole Air Inlet (WAI) with a cut-off size of 30 µm. More detailed explanations on the SMPS and the inlet system can be found in Venzac et al. (2009). Since clusters were previously shown to be very sensitive to the presence of clouds at high-altitude stations (Lihavainen et al., 2007; Venzac et al., 2007), cloudy conditions were filtered out by using RH data. Indeed, cluster ions, and eventually cluster particles, are very efficiently scavenged by the cloud droplets that offer a large condensational sink. Cluster formation and subsequent growth to larger particle sizes would be difficult to follow due to this very high sink. The threshold value RH = 98 % was used to separate in-cloud and out-of-cloud conditions.

## 2.3 Data analysis

### 2.3.1 Sulfuric acid concentration

Sulfuric acid concentrations ([H$_2$SO$_4$]) were calculated using a proxy adjusted on concentrations derived from APi-TOF measurements conducted between 30 January and 6 February 2012 at the PUY (no data available between 10 and 29 February), during which atmospheric conditions, and especially temperatures, were similar to the conditions observed between 10 and 29 February:

$$[H_2SO_4] = k \frac{GlobRad \cdot [SO_2]}{CS \cdot RH}, \tag{1}$$

where $k$ is a scaling factor, and GlobRad is the global radiation in W m$^{-2}$, [SO$_2$] is the sulfur dioxide concentration in molec cm$^{-3}$, CS is the condensation sink in s$^{-1}$ and RH is the relative humidity. The form of Eq. (1) was suggested by Mikkonen et al. (2011) and is based on previous work by Petäjä et al. (2009). This proxy was constructed for radiations higher than 10 W m$^{-2}$ but the predictive ability is significantly raised for radiations exceeding 50 W m$^{-2}$, which was roughly achieved between 07:30 and 16:30 UTC ($-1$ h local time in winter) during the studied period. As previously mentioned, in the present study, the scaling factor $k = 6.0060 \times 10^{-7}$ m$^2$ W$^{-1}$ s$^{-1}$ was empirically obtained by using a linear fitting procedure on sulfuric acid concentrations derived from APi-TOF measurements. After adjusting the proxy, the average positive and negative bias between proxy estimations and the APi-TOF-derived concentrations were $0.57 \times 10^7$ and $-0.97 \times 10^7$ cm$^{-3}$, respectively.

A potential systematic error on the sulfuric acid concentration calculation from the APi-TOF due to an unadapted use of the PUY scaling factor is of course possible, and would affect the absolute values of calculated sulfuric acid concentrations, but not their variability. We thus clearly believe that the accuracy of the proxy derived from Eq. (1) and adjusted on measurements is high enough to study the relative changes in the sulfuric acid concentration from one period to the other.

### 2.3.2 Boundary layer height determination

The estimation of the BL height was derived from LIDAR data and is based on the fact that aerosol concentrations, and thus the LIDAR signal, show a sudden drop between the BL and the FT. The most common used methods are (1) the measurement of the LIDAR signal variance, (2) the measurement of the LIDAR signal gradient and (3) the analysis of the analogy between the LIDAR signal and a wavelet. The last method, called wavelet covariance technique (WCT), appears to be the most relevant (Baars et al., 2008) and was used in the present study. The WCT uses the covariance transform $W$ of the Haar function $h$ (Brooks, 2003):

$$W(a,b) = \frac{1}{a} \int_{z_b}^{z_t} S(z) h\left(\frac{z-b}{a}\right) dz \qquad (2)$$

with

$$h\left(\frac{z-b}{a}\right) = \begin{cases} 1 : b - \frac{a}{2} \leq z \leq b \\ -1 : b \leq z \leq b + \frac{a}{2} \\ 0 : \text{elsewhere} \end{cases} \qquad (3)$$

where $z$ is altitude, $S(z)$ is the LIDAR backscatter profile corrected with $z^2$, the $z_b$ and $z_t$ are the lower and upper limit of the profile, respectively, $b$ is the altitude at which the Haar function is centred and $a$ is the spatial extent. The $a$ was set to $12\Delta r$ according to Baars et al. (2008), where $\Delta r = 7.5$ m is the spatial resolution of the LIDAR.

Equation (3) was applied to all LIDAR profiles with a time resolution of 10 min and for each profile the BL height was identified as the maximum of the $W$ function. These calculations were made under the assumptions that (1) topography does not influence the BL height at the location where the LIDAR measurements take place and (2) aerosol particles are homogeneously mixed within the BL.

LIDAR measurements were previously used by Boulon et al. (2011) to derive BL height at the PUY, but with a calculation method which slightly differs from the WCT. In fact, the WCT aims at finding the upper limit of the aerosol layer, whereas the method developed by Boulon et al. (2011) was designed to find the transition between Mie and Rayleigh diffusion regimes. When applying this last method to our data set, we find BL heights that are very similar to those derived from the WCT, i.e. 8 % higher on average. The reliability of

the LIDAR-derived BL height was also tested and approved by Boulon et al. (2011) using potential equivalent temperature.

### 2.3.3 Particle formation and growth rate calculations

Particle formation and growth rates are key entities to characterize a NPF event, especially in the very first steps of the formation process, i.e. between 1 and 3 nm. As previously mentioned, the PSM was measuring in a scanning mode during the studied period, but the differences between the concentrations of the successive size classes were too small to allow determination of size distributions, and hence any growth rate calculation. Thus we calculated the total particle formation rate at 1.5 nm, $J_{1.5}^{tot}$, from the total particle concentration measured in the size range 1–2.5 nm by the PSM, $N_{1-2.5}$, and by using the growth rates derived from the NAIS in the ion mode in the size range 1.5–3 nm, $GR_{1.5-3}$. GRs were calculated with the "maximum concentration" method originating from Hirsikko et al. (2005). In this method, the time corresponding to the maximum concentration in each size class of the selected size range is first determined by fitting a normal distribution to the size class concentration; the growth rate of the corresponding size range is then obtained by a linear least square fit through the time values previously found. The total particle formation rate at 1.5 nm was finally calculated according to Eq. (4), from Kulmala et al. (2007):

$$J_{1.5}^{tot} = \frac{dN_{1-2.5}}{dt} + CoagS_{1.5} \times N_{1-2.5} + \frac{1}{1.5\,nm} GR_{1.5-3} \times N_{1-2.5}, \qquad (4)$$

where $CoagS_{1.5}$ represents the loss of 1.5 nm particles on larger pre-existing particles from the background size distribution. In the case of charged particles, Eq. (4) is completed by two terms to take into account the loss of ions by recombination and the attachment of ions to neutral particles:

$$J_{1.5}^{\pm} = \frac{dN_{1-2.5}^{\pm}}{dt} + CoagS_{1.5} \times N_{1-2.5}^{\pm} + \frac{1}{1.5\,nm} GR_{1.5-3} \times N_{1-2.5}^{\pm} + \alpha \times N_{1-2.5}^{\pm} N_{<2.5}^{\mp} - \beta \times N_{1-2.5} N_{<1}^{\pm}, \qquad (5)$$

where $N_{1-2.5}^{\pm}$ is the ion number concentration (positive or negative) in the diameter range 1–2.5 nm and $N_{<y}^{\pm}$ is the ion concentration below $y$ nm. The $\alpha$ and $\beta$ are the ion–ion recombination and the ion–neutral attachment coefficient, respectively, and were assumed to be equal to $1.6 \times 10^{-6}$ cm$^3$ s$^{-1}$ and $0.01 \times 10^{-6}$ cm$^3$ s$^{-1}$, respectively (Tammet and Kulmala, 2005).

The smallest particles include both clusters and large molecules, and the exact critical size cannot be known (Kulmala et al., 2013). For that reason, and also to investigate the evolution of the formation rate as a function of cluster size, particle formation rates are usually calculated for different size classes. The formation of 3 nm clusters ($J_3^{tot}$) and ions

$(J_3^\pm)$ was thus analysed by using the cluster concentrations in the size range 3–5 nm and the growth rate over the 3–5 nm diameter range, both derived from NAIS measurements.

## 3 Results and discussion

### 3.1 Charged and neutral cluster concentrations in the free troposphere

#### 3.1.1 Identification of free tropospheric conditions

The study includes 7 days between the 10 and 29 February 2012. Based on a visual analysis of the contour plot of the ion size distribution, five of these days were classified as NPF event days (10, 11, 12, 28 and 29 of February) and the remaining two (21 and 22 February) were considered as non-event days. These days were selected because they were characterized by clear skies and they gave a unique chance to investigate free tropospheric conditions and the interface between the BL and the FT during the first part of the day, i.e. when nucleation and early growth of new particles occur. Such conditions at the station can only be achieved when convective air mass movements are limited. These criteria were fulfilled during a period of exceptionally cold temperatures during winter 2012 in Europe. In the following, the studied data set will be divided into three sub-periods, so that the 10, 11 and 12 will be referred as "Period 1", 21 and 22 as "Period 2" and 28 and 29 as "Period 3".

Figure 1 shows the BL height derived from LIDAR measurements using the WCT method (see Sect. 2.3.2). SMPS particle size distributions (PSD), nitrogen dioxide concentrations ($NO_2$) and wind speed are given as additional information to distinguish between FT and BL in Fig. 2.

During Periods 2 and 3, the BL height rarely exceeds the altitude of the PUY, indicating that the station could be almost continuously above the BL (Fig. 1). However, $NO_2$ concentration starts to increase between 10:30 and 11:00 (UTC, $-1$ h local time in winter) on the 28 and 29, which coincide with the detection of an accumulation mode on the PSD (Fig. 2). These last observations lead to a balance of LIDAR indications and suggest that during Period 3, the measurement site could be located in the FT in the early morning until $\sim 10{:}30$ UTC, and is then progressively influenced by the upper BL. A closer look at the 28 reveals that the total cluster concentration starts to increase around 10:00 UTC, i.e. before $NO_2$ and other BL tracers, such as the relative humidity and the condensation sink (Fig. 3), and reaches its maximum at 11:45 UTC, which suggests that the nucleation process could be initiated in the FT, and then continued in the interface layer between the BL and the FT. In contrast, on the 29 (figure not shown), the beginning of the major cluster concentration increase is seen at 11:30 UTC, i.e. almost 1 h after the beginning of the $NO_2$ augmentation. Thus it is likely that contrary to the 28, on this last day of Period 3 the nucleation

process is most probably triggered at the interface between the BL and the FT rather than in the FT. On the 21, based on LIDAR measurements and PSD, it is likely that the station is located in the BL in early morning and late evening, i.e. outside of the nucleation hours, and in the FT during the rest of the day. On the 22, all measurements agree to conclude that the station is in the FT during the whole day.

In contrast, during Period 1 the BL height displays a clear diurnal variation with a maximum between 1700 and 2000 m a.s.l. around 17:00 UTC. LIDAR measurements suggest that during these days, the PUY could be in the FT until 12:00 UTC and then progressively reached by the BL in the afternoon (Fig. 1). However, on the 10 and the 11, considering the presence of a significant accumulation mode on the PSD (missing data on the 10 are due to an instrument failure), the high $NO_2$ concentrations and the higher variability of wind speed (Fig. 2), it is likely that in the morning, the station is not in the FT but rather at the interface between the BL and the FT. The fact that $NO_2$ concentrations show higher values compared to Period 3 suggests that on the 10 and 11, nucleation hours are most probably characterized by interface/upper BL conditions, whereas interface/FT conditions were found to be predominant on the 28 and 29. On the 12, $NO_2$ concentrations are slightly decreased compared to the previous days, and the accumulation mode also seems to be less intense. These conditions are very similar to the conditions observed during Period 3, suggesting that during the nucleation hours, the station could be in the upper part of the interface layer between the BL and the FT, almost in the FT.

In short, during the selected days, nucleation hours at the station are characterized by upper BL/interface conditions during Period 1, free tropospheric conditions during Period 2 and interface/FT conditions during Period 3, allowing a direct comparison of the events occurring in the different conditions and an investigation of the parameters playing a key role during the different sub-periods.

Previous observations of cluster and aerosol size distributions at high altitudes have rarely shown NPF events occurring in the FT. NPF events at high altitudes were always observed to occur during upwind valley winds (Venzac et al., 2008), or very close to the interface between the BL and the FT (Boulon et al., 2011). The present observations from Period 3, and more especially from the 28 are hence one of the first showing NPF in the FT during clear-sky conditions.

#### 3.1.2 Charged and neutral cluster concentrations

We measured total ($N_{\text{tot}}$) and charged ($N_i$) cluster concentrations in the range 1–2.5 nm mobility diameter, using respectively the PSM and the NAIS. The neutral cluster concentrations ($N_n$) in the same size range were calculated according to $N_n = N_{\text{tot}} - N_i$. Figure 4 shows the mean diurnal variation of total and charged cluster concentrations, separately for the three sub-periods. In agreement with previous observations at the site (Manninen et al., 2009; Boulon et al., 2011;
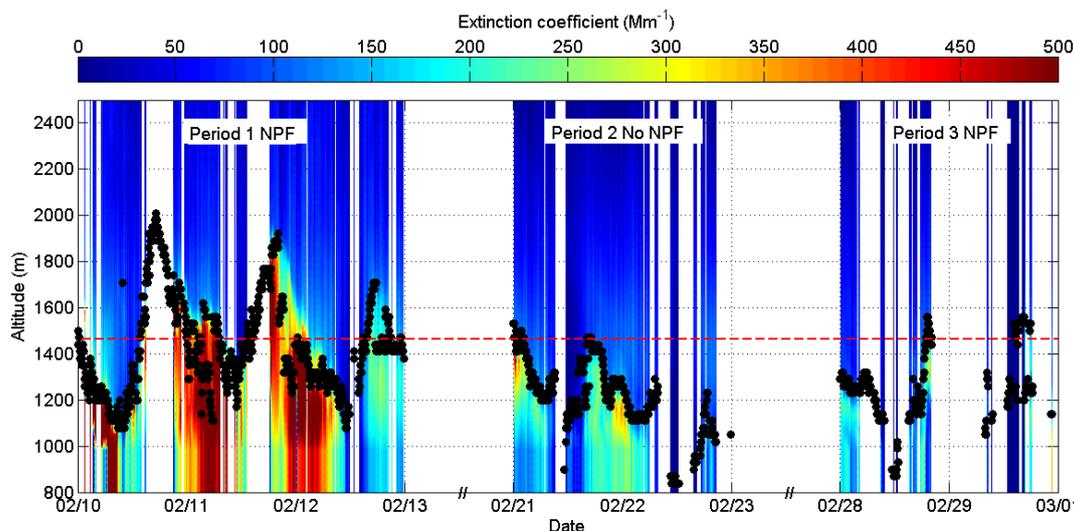
**Figure 1.** Boundary layer height determination from LIDAR measurements. In the present study, boundary layer (BL) height (black dots) is assumed to be equal to the aerosol mixing layer height and was calculated using the WCT method. Red dashed line represents the altitude of the station (1465 m a.s.l). The presence of high-altitude clouds or frost on the instrument avoids both the extinction coefficient and the BL height calculations. However, when clouds are detected at the altitude of the station, the values of the extinction calculation remain unreliable but a correct estimation of the BL height is allowed. The occurrence of NPF during the sub-periods defined in Sect. 3.1 is indicated at the top of the figure. February 2012, Puy de Dôme.

**Table 1.** Cluster concentrations for each sub-period. Median, 25th and 75th percentiles of charged cluster concentration ($N_i$), total cluster concentration ($N_{tot}$) and neutral cluster concentration ($N_n$) during the different periods. The indices day refer to values calculated over the whole day whereas the indices nucl refer to values calculated during the time period 10:30–14:00 (UTC). Indication <LDL refers to concentrations below the lower detection limit (500 cm$^{-3}$) that was set for the total cluster concentration measured by the PSM; corresponding neutral cluster concentrations which are negative are not reported. The occurrence of NPF during the sub-periods is shown in the table. February 2012, Puy de Dôme.

| | Period 1 NPF | | | Period 2 No NPF | | | Period 3 NPF | | |
|---|---|---|---|---|---|---|---|---|---|
| | Med. | 25th perc. | 75th perc. | Med. | 25th perc. | 75th perc. | Med. | 25th perc | 75th perc |
| $N_{i\_day}$(cm$^{-3}$) | 275.0 | 187.6 | 391.9 | 651.5 | 563.3 | 690.0 | 752.3 | 681.3 | 802.8 |
| $N_{i\_nucl}$(cm$^{-3}$) | 473.1 | 392.8 | 533.2 | 656.1 | 594.1 | 694.5 | 714.8 | 657.2 | 757.3 |
| $N_{tot\_nucl}$(cm$^{-3}$) | 2049.1 | 821.9 | 7265.1 | <LDL | <LDL | <LDL | 921.4 | 715.8 | 1354.8 |
| $N_{n\_nucl}$(cm$^{-3}$) | 2022.9 | 453.7 | 6765.0 | – | – | – | 281.4 | 7.4 | 854.0 |

Rose et al., 2013) cluster ions appear to be present on both event and non-event days. Charged cluster concentrations are on average higher during Periods 2 and 3, when the station is more frequently disconnected from the BL compared to Period 1 (factor of 1.5 between Periods 1 and 3). Charged cluster concentrations do not show any clear diurnal variations, with the exception of the positive cluster ions which exhibit higher concentrations around 12:00 UTC during Period 1. This observation is supported by the values reported in Table 1: the median concentration calculated from the nucleation hours (10:30–14:00 UTC) is increased by a factor of 1.72 compared to the median calculated over the whole day during Period 1. This behaviour of positive ions was previously observed by Rose et al. (2013), who reported that positive cluster ion concentrations were increased during NPF

events over a 5 yr long study. The contrasting behaviour of positive ions observed during Period 3 might be explained by the unusual atmospheric conditions – especially low temperatures and free tropospheric conditions (Figs. 1, 2, 4a). Positive cluster ion concentrations always exceed negative cluster concentrations, especially during Period 2 (factor 3.23). This trend differs from the results of the long-term study by Rose et al. (2013) and might again be eventually explained by the atmospheric conditions observed in February 2012.

In contrast to the behaviour of cluster ions, the total cluster concentration displays very different trends and values on event days compared to non-event days (Fig. 3). On non-event days, the total cluster concentration does not significantly vary with the time of the day and is almost continuously below the cluster ion concentration. This last observa-
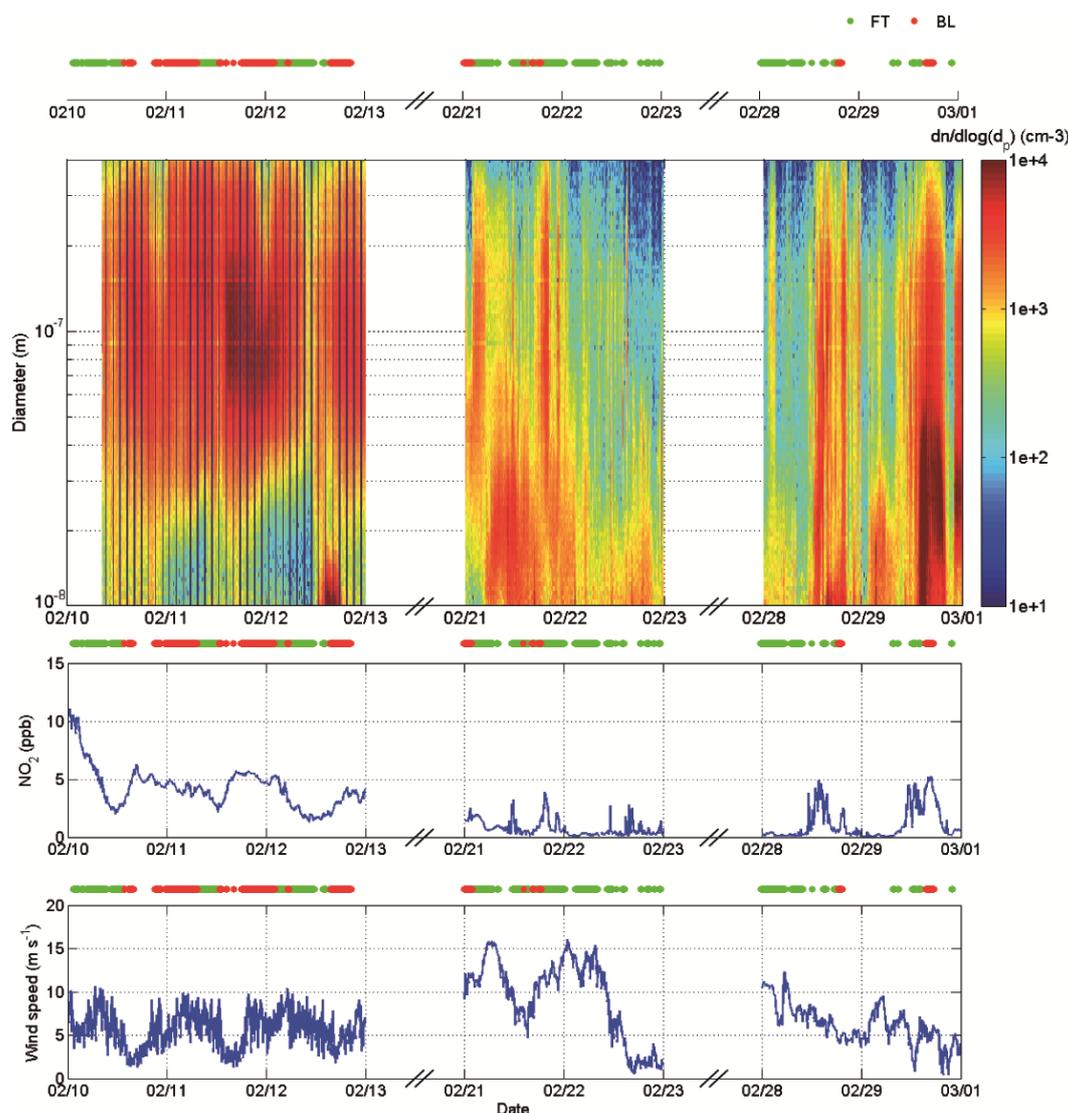
**Figure 2.** SMPS particle size distribution, $NO_2$ concentrations and wind speed measurement used as additional information to distinguish between the BL and the FT.

tion supports the fact that the PSM could be unable to detect all of the cluster ions, most likely because of their chemical composition (Kangasluoma et al., 2013; Wimmer et al., 2013). In the present study, we observed that for ion concentrations below $\sim 500\,\mathrm{cm}^{-3}$, the total cluster concentration measured by the PSM was systematically lower than the ion concentration, leading to non-physical negative values for the neutral cluster concentration. There is no correction for this artefact, as it depends on the chemical composition of the clusters, which is unknown during nucleation events. In order to remain physically correct but avoid overestimating the total cluster concentration, we decided to introduce a lower detection limit (LDL) of $500\,\mathrm{cm}^{-3}$ for total cluster concentrations and to filter out all the total cluster concentrations that were below this limit. Hence, the total cluster concen-

trations that we report in this work are a lower limit of the actual total cluster concentrations.

On event days, the total cluster concentration exhibits a very clear diurnal variation with a maximum detected between 10:30 and 14:00 UTC. One should note that these maxima significantly vary from day to day, since the median total cluster concentration calculated during the nucleation hours of Period 1 is more than doubled compared to Period 3 (Table 1). This last observation is mainly explained by the low concentrations observed on the 28, during which nucleation hours were most probably characterized by interface/FT conditions, suggesting that the formation of neutral clusters could be less intense in the FT compared to interface/BL conditions. This last point will be further discussed in the next sections.
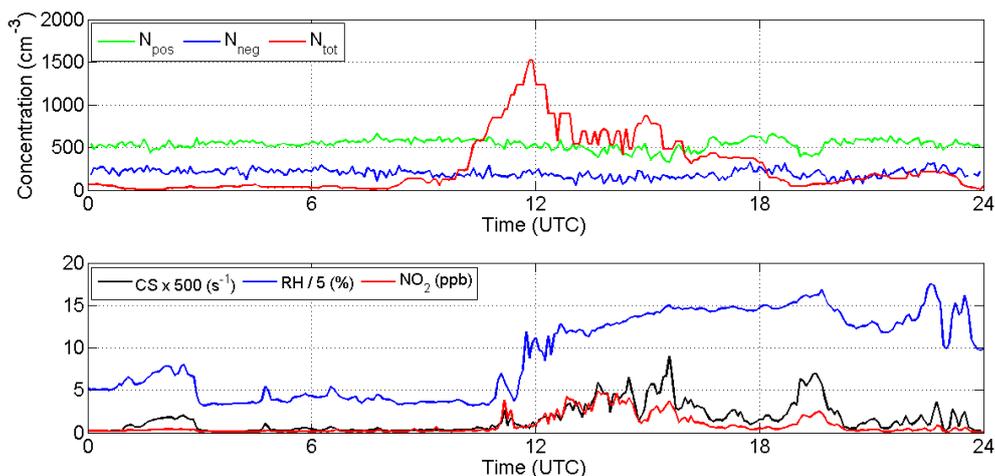
**Figure 3.** Diurnal variation of the cluster concentrations (upper panel) and BL tracers (lower panel: condensation sink (CS), relative humidity (RH) and $NO_2$) observed at the PUY on 28 February.
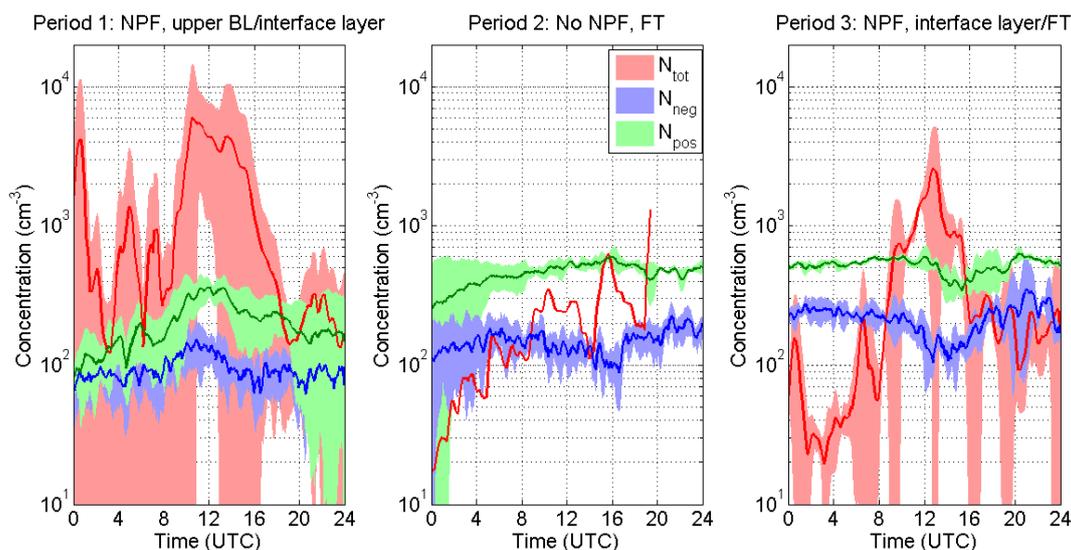


**Figure 4.** Mean diurnal variation of positive ($N_{pos}$), negative ($N_{neg}$) and total ($N_{tot}$) clusters (1 to 2.5 nm mobility diameter) during the three sub-periods. Lower and upper limits of the shaded areas represent the standard deviation of the corresponding concentration. On non-event days, the lack in total cluster concentration measurement is due to an instrument failure. The occurrence of NPF during the sub-periods as well as the location of the station during nucleation hours are indicated at the top of the figure. February 2012, Puy de Dôme.

The observed diurnal variation of the cluster concentration can be explained by the formation of clusters during the nucleation process in the morning and their growth and/or removal on pre-existing particles in the afternoon. During the nucleation hours, the total cluster concentration more frequently exceeds the charged cluster concentration, clearly indicating the formation of neutral clusters. In particular, averaged neutral cluster concentrations exceed the charged cluster concentration by a factor of 4.3 during Period 1, and the charged fraction $f = N_i / N_{tot}$ is close to 0.23 during the nucleation peak. During Period 3, neutral clusters are also clearly increased during the nucleation process, but the

charged fraction is significantly higher compared to Period 1 (0.78), suggesting again that the efficiency of neutral pathways could be less important when free tropospheric conditions are predominant. Outside of the nucleation hours, total cluster concentrations are below the charged cluster concentration, being very similar to the concentrations recorded on non-event days during Period 2.

The continuous presence of cluster ions has already been reported by several studies at ground stations, both at low (Manninen et al., 2009) and at high altitude (Boulon et al., 2010; Rose et al., 2013) and the diurnal variation of the charged cluster concentration on event days was also ob-

served at several stations (Hõrrak et al., 2008; Boulon et al., 2010; Rose et al., 2013). According to recent studies, neutral clusters also seem to be ubiquitous in the atmosphere (Lehtipalo et al., 2009, 2010). Kulmala et al. (2013) reported a continuous presence of sub-2.1 nm neutral clusters in Hyytiälä, Finland, with concentrations in the range 500–20 000 cm$^{-3}$. In Finokalia, Greece, sub $-2.5$ nm total cluster concentrations were in the range 10–10 000 cm$^{-3}$, with lower values at night. NAIS airborne measurements from the whole tropospheric column (up to 12 km) conducted in the frame of the EUCAARI–LONGREX campaign (May 2008) were reported by Mirme et al. (2010) and showed similar results. In fact, charged clusters were continuously detected at all altitudes with a mode centred around 1 nm. Between 2.5 and 3 nm, total cluster concentrations significantly exceeded charged concentrations, suggesting a continuous pool of sub-3 nm neutral clusters throughout the whole tropospheric column.

The observations reported in this section suggest that at the PUY, differences between the charged and total cluster concentrations are significant enough to conclude that the formation of neutral clusters dominates the formation of total clusters during NPF events occurring at the interface between the BL and the FT, as well as in the FT. Contrarily to airborne measurements, high-altitude ground-based measurement offers the possibility to study particle formation and growth rates.

### 3.1.3 Particle formation and growth rates

Particle formation and growth rates are given in Table 2 for each event day. The formation rates exhibit significant variations from one event to the other. One can notice that the charged formation rates of positive 1.5 nm clusters are significantly higher than the charged formation rates of negative 1.5 nm clusters, and that the difference is more pronounced during Period 3 (factor of 6.8 compared to 2.4 during Period 1). Similar observations were reported in the CLOUD (Cosmics Leaving Outdoor Droplets) experiment (Kirkby et al., 2011), which studied the role of sulfuric acid, ammonia and ions in the nucleation process. In particular, the occurrence of ternary nucleation involving sulfuric acid at high ammonia mixing ratios, with typical path on positive way, could explain the excess of positive ions, at least on event days. Moreover, the average formation rates of total 1.5 nm particles exceed those of charged particles, especially during Period 1 which displays ion-induced nucleation fractions (IIN) lower than 4.3 % ($J_{1.5}^{tot} \approx 37 \times J_{1.5}^{+}$ and $J_{1.5}^{tot} \approx 77 \times J_{1.5}^{-}$), which is relatively low compared to the average values reported for altitude sites (Boulon et al., 2010; Manninen et al., 2010), and especially for the PUY (12.5 ± 2.0 %, Boulon et al., 2011). In contrast, the IIN rates are higher during Period 3, with a value close to 50 % on the 28 February, suggesting that charged pathways could be promoted in the FT compared to the interface between the BL and the FT. How-

ever, besides the height of the BL itself, atmospheric parameters such as temperature and relative humidity display significant variations between the different periods, and could also explain the previous observations (Table 3 and Fig. 5). This potential effect is further discussed in Sect. 3.2.4.

In can be seen from Table 2 that the formation rates of charged and neutral 3 nm particles are significantly decreased compared to the formation rates of charged and neutral 1.5 nm clusters, which is due to the loss of small particles by coagulation on bigger pre-existing particles during their growth.

GR values also experience significant variations between the different events, with a maximum-to-minimum ratio of 8.7 for GR$_{1.5-3}$ and 4.3 for GR$_{3-5}$. Particularly, on the 12 and 29, which correspond to the strongest particle formation events of the two sub-periods, GR$_{1.5-3}$ displays values larger than 10 nm h$^{-1}$. In contrast with the particle formation rate, the particle growth rate is on average increasing as a function of particle size (Table 2), suggesting the participation of other vapours than sulfuric acid (Kuang et al., 2012b; Kulmala et al., 2013).

The results we obtain clearly suggest that in the FT, and even more at the interface between the BL and the FT, the formation of neutral clusters dominates the formation of total clusters during NPF events. This observation goes in the same direction as Lehtipalo et al. (2010) and Kulmala et al. (2013) who observed a very small contribution of ions in the dynamics of sub-2 nm clusters during the nucleation process at the BL site of Hyytiälä. Indeed, both the concentrations of sub-2 nm clusters and the formation rate of 1.5 nm clusters were found to be clearly dominated by neutral particles, sometimes with differences exceeding several orders of magnitude. $J_{1.5}^{tot}$ values reported for Hyytiälä are similar to the values obtained at the PUY, with maximum values around 5 cm$^{-3}$ s$^{-1}$ at 12:00 UTC. In contrast, $J_{1.5}^{\pm}$ exhibits slightly lower values in Hyytiälä, being in the range $3 \times 10^{-2} - 6 \times 10^{-2}$ cm$^{-3}$ s$^{-1}$. This observation is in agreement with the previous observations by Boulon et al. (2010) and Manninen et al. (2010) who suggested that charged nucleation pathways could be promoted at higher altitudes compared to low altitudes.

The purpose of the following section is now to investigate the atmospheric conditions that could favour the occurrence of NPF observed during the different periods and their link to cluster concentrations.

### 3.2 Analysis of the atmospheric conditions promoting particle formation at the BL/FT interface and in the FT

As previously mentioned, among the 7 studied days, 5 were identified as event days and the remaining 2 as non-event days. We further investigated the changes in atmospheric conditions which lead or not to NPF during this period. For this purpose, several parameters were analysed in addition

**Table 2.** Summary of the particle formation event characteristics. $GR_{1.5-3}$ and $GR_{3-5}$ are the particle growth rates in 1.5–3 and 3–5 nm size ranges respectively, $J_{1.5}^{\pm}$ and $J_3^{\pm}$ are ion formation rates at 1.5 and 3 nm and $J_{1.5}^{\text{tot}}$ and $J_3^{\text{tot}}$ are the corresponding total particle formation rates during the event. Instruments used for the calculation of each parameter are specified in the third row; for the NAIS also the mode used for the measurements is given. February 2012, Puy de Dôme.

| Date | $GR_{1.5-3}$ $(\text{nm h}^{-1})$ | $GR_{3-5}$ | $J_{1.5}^{+}$ | $J_{1.5}^{-}$ $(\text{cm}^{-3}\,\text{s}^{-1})$ | $J_3^{+}$ | $J_3^{-}$ | $J_{1.5}^{\text{tot}}$ $(\text{cm}^{-3}\,\text{s}^{-1})$ | $J_3^{\text{tot}}$ |
|---|---|---|---|---|---|---|---|---|
| | NAIS ion | | | NAIS ion | | | PSM | NAIS particle |
| 10 Feb | 1.65 | 8.45 | $0.084 \pm 0.057$ | $0.025 \pm 0.033$ | $0.049 \pm 0.044$ | $0.062 \pm 0.050$ | $2.87 \pm 3.71$ | $1.38 \pm 0.91$ |
| 11 Feb | 1.93 | 3.58 | – | $0.010 \pm 0.030$ | – | $0.013 \pm 0.009$ | $0.58 \pm 0.64$ | $0.34 \pm 0.23$ |
| 12 Feb | 14.36 | 15.57 | $0.468 \pm 0.083$ | $0.311 \pm 0.100$ | $0.139 \pm 0.071$ | $0.245 \pm 0.147$ | $18.24 \pm 10.11$ | $2.20 \pm 0.94$ |
| 28 Feb | 1.90 | – | $0.183 \pm 0.067$ | $0.022 \pm 0.027$ | – | – | $0.42 \pm 0.28$ | – |
| 29 Feb | 10.45 | 5.06 | $0.686 \pm 0.148$ | $0.132 \pm 0.070$ | $0.011 \pm 0.011$ | $0.011 \pm 0.012$ | $4.32 \pm 2.84$ | $0.60 \pm 0.58$ |

**Table 3.** Summary of the mean values of several atmospheric parameters for each sub-period. The occurrence of NPF during the sub-periods is indicated in the table. February 2012, Puy de Dôme.

| | Period 1 NPF | Period 2 no NPF | Period 3 NPF |
|---|---|---|---|
| $T$ (°C) | $-14.24$ | $-1.40$ | $4.96$ |
| RH ( %) | 90.80 | 29.32 | 51.8 |
| BC ( $\text{ng m}^{-3}$) | 687.53 | 87.83 | No data |
| CS ($\text{s}^{-1}$) | $1.36 \times 10^{-2}$ | $1.60 \times 10^{-3}$ | $2.40 \times 10^{-3}$ |
| CO (ppb) | 210.78 | 126.29 | 119.86 |
| $H_2SO_4$ ($\text{molec cm}^{-3}$) | $0.72 \times 10^7$ | $9.14 \times 10^7$ | $2.79 \times 10^7$ |

to BL height, including temperature, relative humidity (RH), black carbon concentration, carbon monoxide concentration (CO), as well as condensation sink (CS) and sulfuric acid concentration ($H_2SO_4$), and are presented in Table 3 and Fig. 5. Three-day air mass back trajectories (calculated from the HYSPLIT transport and dispersion mode, Draxler and Rolph, 2003) are also shown in Fig. 6.

### 3.2.1 Description of the atmospheric conditions in each sub-period

As previously mentioned, during Period 1 the PUY was most probably located at the interface/upper BL in the morning and in the BL during the second part of the day (Figs. 1 and 2). Consequently, Period 1 is characterized by high RH (on average 90.8 %) (Fig. 5b and Table 3) and displays the highest BC and CO concentrations, with average values of $687.53\ \text{ng m}^{-3}$ and 210.78 ppb, respectively (Fig. 5c and d). This relatively high level of pollution for the site might in addition also be explained by air masses coming from eastern Europe, especially on the 11 (Fig. 6). High emissions can originate from biomass and fuel burning from intensive domestic heating due to very cold temperatures occurring during this period, which never exceed $-12\,°C$ at the PUY, being on average $-14.2\,°C$ (Fig. 5a). The condensation sink is logically well correlated with BC concentrations and displays the highest average value ($1.36 \times 10^{-2}\ \text{s}^{-1}$) of the three sub-periods (Fig. 5e). In contrast, sulfuric acid concentrations are

the lowest of the entire measurement period, with an average value of $0.72 \times 10^7\ \text{molec cm}^{-3}$ (Fig. 5f).

During Period 2, the BL height rarely reaches the altitude of the station, suggesting that the PUY is hardly influenced by BL direct emissions (Figs. 1 and 2). As a consequence, average RH is decreased to 29.3 % and BC and CO concentrations are also significantly lower compared to Period 1, with typical values in the range $70$–$420\ \text{ng m}^{-3}$ and $100$–$158$ ppb, respectively (Fig. 5c and d). Beside the lower altitude of the BL height relative to the site, these lower concentrations may be partly attributed to the geographical origin of air masses reaching the PUY that have turned from the northern Europe sector (Fig. 6), and which have already been reported to be less polluted than eastern air masses (Venzac et al., 2009; Bourcier et al., 2012). Finally, temperatures are higher during Period 2 compared to Period 1 (Fig. 5a), which may also lead to less domestic heating and thus lower pollution originating from combustion processes. Consequently, we observe that the condensation sink is also decreased and displays the lowest values of the whole studied period, being on average $1.60 \times 10^{-3}\ \text{s}^{-1}$ (Fig. 5e). At the same time, sulfuric acid concentrations are increased compared to Period 1, being the highest of the three sub-periods (Fig. 5f).

The last period, referred to as Period 3, includes the 28 and 29 February. Period 3 is characterized by the same BL heights as Period 2 (Figs. 1 and 2) but both RH, CO concentrations and CS (no information concerning BC concentrations because of instrument failure) are slightly higher
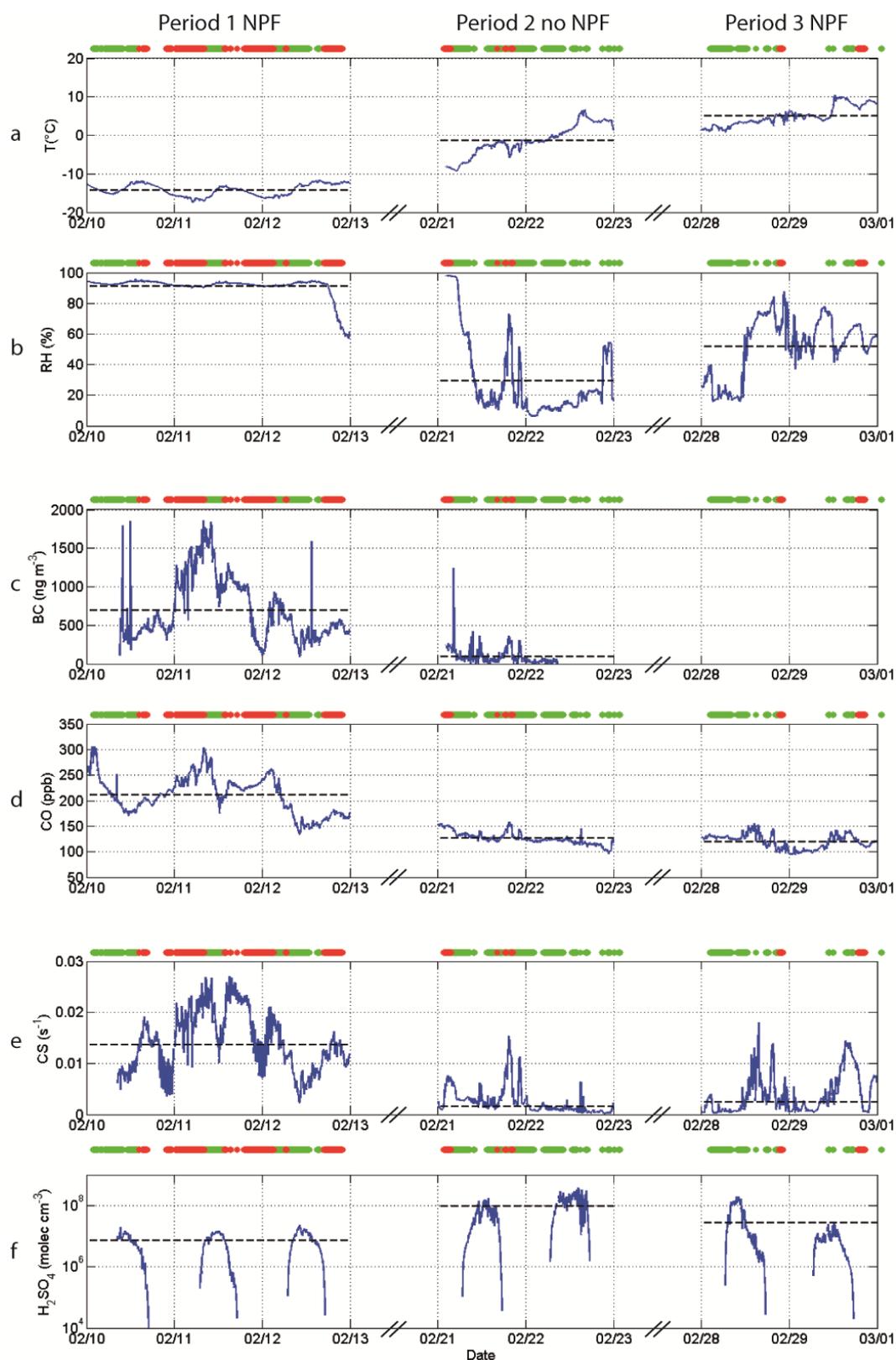
**Figure 5.** Overview of atmospheric parameters during the studied period. Black dashed lines represent the mean value of each parameter during the three sub-periods. The occurrence of NPF during the sub-periods as well as the location of the station in the BL (red) or in the FT (green) are indicated at the top of the figure. February 2012, Puy de Dôme.
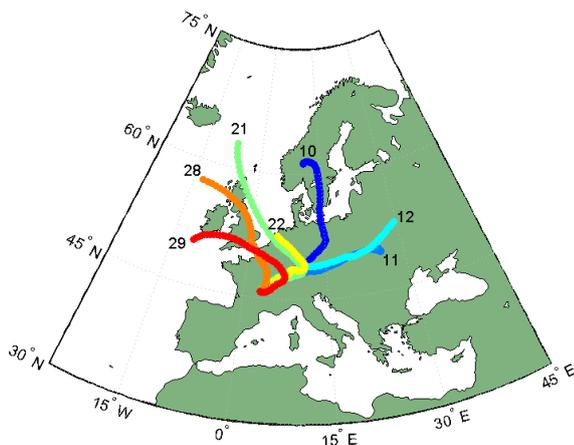
**Figure 6.** Three-day back trajectories of air masses reaching the Puy de Dôme at 12:00 UTC. Days are indicated on the map close to the corresponding trajectories.

than during Period 2, with average values of 51.8 %, $2.4 \times 10^{-3} \, \text{s}^{-1}$ and 119.86 ppb, respectively (Table 3). Nonetheless, it is worth noting that they remain broadly lower than during Period 1. During Period 3 temperatures continue to increase, so that the contribution of combustion sources to the condensation sink is likely further decreased (Fig. 5a). However, during Period 3, air masses originate from the northeast part of Europe and they cross the United Kingdom before reaching the PUY (Fig. 6). Thus they are more polluted than the air masses arriving during Period 2. Sulfuric acid concentrations appear to be significantly lower than during Period 2, with an average value of $2.79 \times 10^7 \, \text{molec cm}^{-3}$ (Fig. 5f).

### 3.2.2 The role of sulfuric acid

Based on Fig. 5, Tables 1 and 3, we can first assert that $H_2SO_4$ is not the main driver of the nucleation process at the PUY – not at the interface between the BL and the FT nor in the FT. Indeed, despite the fact that Period 2 is characterized by the highest sulfuric acid concentrations, no NPF events were detected during these days. Note that similar conclusions are obtained when using proxies for the sulfuric acid concentration that includes scaling factors from the literature, such as the ones proposed in Petäjä et al. (2009) or Mikkonen et al. (2011).

Also, there is no clear correlation between cluster concentrations and sulfuric acid, as illustrated by Fig. 7a. In particular, sulfuric acid concentrations obtained during Period 1 are on average 3.9 times lower than during Period 3, whereas median neutral cluster concentration is almost 10 times higher during the nucleation hours of Period 1. This observation supports the analysis of Boulon et al. (2010, 2011) who reported that at high-altitude stations such as the PUY and the Jungfraujoch, Switzerland, gaseous precursors other than sulfuric acid were also involved in the formation and early growth of the clusters into new particles.

### 3.2.3 Influence of the condensation sink

The second important result highlighted by Tables 1–3 is that the occurrence of NPF does not seem to be limited by the condensation sink. In fact, NPF is triggered during Periods 1 and 3, which display CS values significantly higher compared to Period 2. This observation contradicts the previous result by Boulon et al. (2011) at the PUY for ionic clusters but supports the results reported at the Jungfraujoch station (Boulon et al., 2010). However, based on Fig. 7b, we observe that while cluster concentrations are not deeply impacted by the CS up to $\sim 7 \times 10^{-3} \, \text{s}^{-1}$, they seem to decrease with an increasing CS above this threshold value, suggesting that high CS values do not inhibit the nucleation process but could limit the number of nucleated clusters.

In the present study it is likely that condensable compounds involved in the NPF process and condensation sink share the same origin. Gaseous precursors other than sulfuric acid could be oxidized volatile organic compounds, as suggested by several studies (Metzger et al., 2010; Paasonen et al., 2010; Wang and Wexler, 2013). This would explain the fact that during Period 2, which is characterized by dominant free tropospheric conditions and lowest condensation sinks, particle formation is not triggered because of a lack of other gaseous precursors. Thus, our observations suggest that particle formation occurs when the pool of gaseous precursors is supplied to the upper troposphere by inputs of more polluted air masses from the BL. Thus, it is likely that in the lower part of the interface between the BL and the FT (Period 1), particle formation, and especially neutral pathways, are enhanced compared to Period 3 (upper interface layer/FT) thanks to an increased amount of gaseous precursors directly coming from the BL. Similar observations were reported by Neitola et al. (2011) at a high-altitude Indian Himalayan site (2180 m a.s.l.).

### 3.2.4 A potential additional effect of temperature and relative humidity?

In the present study, the occurrence of nucleation and the concentration of nucleated clusters have been discussed so far in terms of sulfuric acid concentration and condensation sink only. However, temperature and relative humidity display significant variations in the course of the measurement period and were previously reported in the literature to have effect on the occurrence of nucleation and on the characteristics of the events (formation rates, cluster concentrations). In fact, low temperatures could favour nucleation, and could in particular explain, together with low CS, the occurrence of NPF in the FT and in the low stratosphere (Young et al., 2007). In contrast, the role of the RH appears to be more equivocal. Numerous observations suggest that nucleation could be favoured at low RH (e.g. Birmili et al., 2003) and both the cluster formation rates (Sihto et al., 2006) and the concentration of freshly formed particles (Jeong et
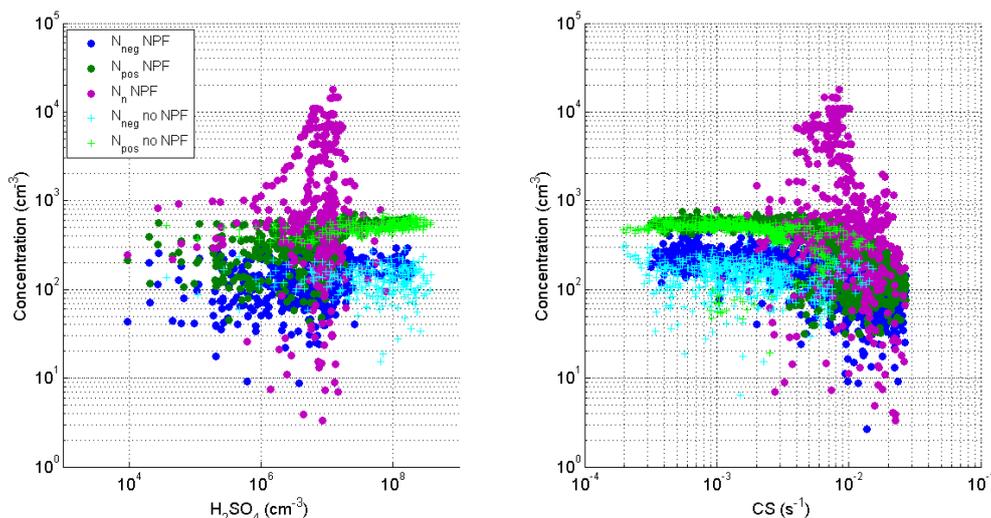
**Figure 7.** Nanoparticle concentrations as a function of potential nucleation source and sink. Positive ($N_{pos}$), negative ($N_{neg}$) and neutral cluster ($N_n$) concentrations as a function of **(a)** sulfuric acid concentration and **(b)** condensation sink are reported separately, for NPF event and non-event days. Neutral cluster concentrations which are negative on non-event days are not shown on the figure. February 2012, Puy de Dôme.

al., 2004) have been reported to be anticorrelated with RH. Nonetheless, NPF events have been observed in the vicinity of clouds, where RH often exceeds 90 % (Clarke et al., 1998). In a more recent study based on model simulations, Hamed et al. (2011) suggest that high RH impacts the amount of solar radiation, and thus the source of condensable species, rather than the sink term.

Thus, it is likely that at the PUY, the very low temperatures measured during Period 1 (average $-14.24\,°C$) could explain, at least partly, the occurrence of nucleation, and maybe the intensive formation of neutral clusters compared to Period 3. However, regarding previous observations from the literature, one could have expected fewer intense NPF events since high RH was simultaneously recorded during Period 1 (90.8 %). The opposite trend is observed for the second NPF period, Period 3, which displays increased temperatures ($4.96\,°C$) and decreased RH (51.8 %) compared to Period 1. During Period 2, RH is further decreased (29.3 %) and temperatures remain low ($-1.40\,°C$), but despite these conditions, which should, on a first approach, be favourable to nucleation, no event is detected.

The previous observations suggest that atmospheric parameters, including temperature, RH, but also sources and sinks, cannot be considered separately. This might be explained by the fact that their effects combine with each other, but the amount of data used in the present study seems to be too small to analyse such combinations or to disentangle the effects of all parameters unambiguously.

## 4   Conclusions

We investigated the charged and neutral cluster concentrations (1–2.5 nm) during NPF events observed to occur at the interface between the BL and the FT and in the FT at the PUY station, during a period characterized by very low temperatures in Europe.

Cluster ions were always present and their concentrations did not exhibit any clear diurnal variation. In contrast, on event days, the total cluster concentration clearly peaked between 10:30 and 14:00 (UTC), with on average higher concentrations during Period 1 (interface/upper BL) than during Period 3 (interface/FT). Total and charged formation rates at 1.5 nm ($J_{1.5}^{tot}$ and $J_{1.5}^{\pm}$ respectively) were derived from PSM and NAIS respectively. The formation rate of positive clusters was higher than the one of negative clusters, especially during Period 3. $J_{1.5}^{tot}$ significantly exceeded $J_{1.5}^{\pm}$, particularly during Period 1, suggesting that neutral clusters were clearly driving the first steps of the NPF process at the PUY in the FT, and even more at the interface between the BL and the FT.

When investigating the atmospheric conditions promoting nucleation during the studied period, we found that sulfuric acid was not the main species driving the nucleation and early growth process since there was no clear link between sulfuric acid and the cluster concentrations, nor between sulfuric acid and the occurrence of NPF. The increasing growth rate of clusters with size supports the observation of sulfuric acid not being the only contributor to early particle growth. Finally, NPF events were detected when the highest condensation sinks were obtained, during Period 1 when the station was in the lower part of the interface between the BL

and the FT, suggesting that gaseous precursors other than sulfuric acid could share the same origin as the condensation sink. According to our observations, it is likely that in the upper troposphere, particle formation would be favoured when the amount of gaseous precursors available for nucleation and early growth is supplied by inputs of more polluted air masses. Temperature and RH might also influence the occurrence of nucleation but the studied data set seems to be too small to distinguish between the effects of the different parameters.

Edited by: K. Lehtinen

# References

Asmi, E., Sipilä, M., Manninen, H. E., Vanhanen, J., Lehtipalo, K., Gagné, S., Neitola, K., Mirme, A., Mirme, S., Tamm, E., Uin, J., Komsaare, K., Attoui, M., and Kulmala, M.: Results of the first air ion spectrometer calibration and intercomparison workshop, Atmos. Chem. Phys., 9, 141–154, doi:10.5194/acp-9-141-2009, 2009.

Baars, H., Ansmann, A., Engelmann, R., and Althausen, D.: Continuous monitoring of the boundary-layer top with lidar, Atmos. Chem. Phys., 8, 7281–7296, doi:10.5194/acp-8-7281-2008, 2008.

Birmili, W., Berresheim, H., Plass-Dülmer, C., Elste, T., Gilge, S., Wiedensohler, A., and Uhrner, U.: The Hohenpeissenberg aerosol formation experiment (HAFEX): a long-term study including size-resolved aerosol, H2SO4, OH, and monoterpenes measurements, Atmos. Chem. Phys., 3, 361–376, doi:10.5194/acp-3-361-2003, 2003.

Boulon, J., Sellegri, K., Venzac, H., Picard, D., Weingartner, E., Wehrle, G., Collaud Coen, M., Bütikofer, R., Flückiger, E., Baltensperger, U., and Laj, P.: New particle formation and ultrafine charged aerosol climatology at a high altitude site in the Alps (Jungfraujoch, 3580 m a.s.l., Switzerland), Atmos. Chem. Phys., 10, 9333–9349, doi:10.5194/acp-10-9333-2010, 2010.

Boulon, J., Sellegri, K., Hervo, M., Picard, D., Pichon, J.-M., Fréville, P., and Laj, P.: Investigation of nucleation events vertical extent: a long term study at two different altitude sites, Atmos. Chem. Phys., 11, 5625–5639, doi:10.5194/acp-11-5625-2011, 2011.

Bourcier, L., Sellegri, K., Chausse, P., Pichon, J. M., and Laj, P.: Seasonal variation of water-soluble inorganic components in aerosol size-segregated at the puy de Dôme station (1,465 m a.s.l.), France, J. Atmos. Chem., 69, 47–66, doi:10.1007/s10874-012-9229-2, 2012.

Brooks, I. M.: Finding Boundary Layer Top: Application of a Wavelet Covariance Transform to Lidar Backscatter Profiles, J. Atmos. Ocean. Tech., 20, 1092–1105, doi:10.1175/1520-0426(2003)020<1092:FBLTAO>2.0.CO;2, 2003.

Clarke, A. D., Varner, J. L., Eisele, F., Mauldin, R. L., Tanner, D., and Litchy, M.: Particle production in the remote marine atmosphere: Cloud outflow and subsidence during ACE 1, J. Geophys. Res.-Atmos., 103, 16397–16409, doi:10.1029/97JD02987, 1998.

Draxler, R. R. and Rolph, G. D.: HYSPLIT (Hybrid Single-Particle Langrangian Integrated Trajectory) Model access via NOAA ARL READY website, available at: http://www.arl.noaa.gov/ready/hysplit4.html (last access: 15 January 2015), 2003.

Eisele, F. L.: Natural and anthropogenic negative ions in the troposphere, J. Geophys. Res.-Atmos., 94, 2183–2196, 1989.

Freney, E. J., Sellegri, K., Canonaco, F., Boulon, J., Hervo, M., Weigel, R., Pichon, J. M., Colomb, A., Prévôt, A. S. H., and Laj, P.: Seasonal variations in aerosol particle composition at the puy-de-Dôme research station in France, Atmos. Chem. Phys., 11, 13047–13059, doi:10.5194/acp-11-13047-2011, 2011.

Hamed, A., Korhonen, H., Sihto, S.-L., Joutsensaari, J., Järvinen, H., Petäjä, T., Arnold, F., Nieminen, T., Kulmala, M., Smith, J. N., Lehtinen, K. E. J., and Laaksonen, A.: The role of relative humidity in continental new particle formation, J. Geophys. Res., 116, D03202, doi:10.1029/2010JD014186, 2011.

Hari, P. and Kulmala, M.: Station for measuring ecosystem-atmosphere relations, Boreal Environ. Res., 10, 315–322, 2005.

Hervo, M., Quennehen, B., Kristiansen, N. I., Boulon, J., Stohl, A., Fréville, P., Pichon, J.-M., Picard, D., Labazuy, P., Gouhier, M., Roger, J.-C., Colomb, A., Schwarzenboeck, A., and Sellegri, K.: Physical and optical properties of 2010 Eyjafjallajökull volcanic eruption aerosol: ground-based, Lidar and airborne measurements in France, Atmos. Chem. Phys., 12, 1721–1736, doi:10.5194/acp-12-1721-2012, 2012.

Hirsikko, A., Laakso, L., Hõrrak, U., Aalto, P. P., Kerminen, V.-M., and Kulmala, M.: Annual and size dependent variation of growth rates and ion concentrations in boreal forest, Boreal Env. Res. 10, 357–369, 2005.

Hõrrak, U., Aalto, P. P., Salm, J., Komsaare, K., Tammet, H., Mäkelä, J. M., Laakso, L., and Kulmala, M.: Variation and balance of positive air ion concentrations in a boreal forest, Atmos. Chem. Phys., 8, 655–675, doi:10.5194/acp-8-655-2008, 2008.

Jeong, C.-H., Hopke, P. K., Chalupa, D., and Utell, M.: Characteristics of Nucleation and Growth Events of Ultrafine Particles Measured in Rochester, NY, Environ. Sci. Technol., 38, 1933–1940, doi:10.1021/es034811p, 2004.

Jokinen, T., Sipilä, M., Junninen, H., Ehn, M., Lönn, G., Hakala, J., Petäjä, T., Mauldin III, R. L., Kulmala, M., and Worsnop, D. R.: Atmospheric sulphuric acid and neutral cluster measurements using CI-APi-TOF, Atmos. Chem. Phys., 12, 4117–4125, doi:10.5194/acp-12-4117-2012, 2012.

Junninen, H., Ehn, M., Petäjä, T., Luosujärvi, L., Kotiaho, T., Kostiainen, R., Rohner, U., Gonin, M., Fuhrer, K., Kulmala, M., and Worsnop, D. R.: A high-resolution mass spectrometer to measure atmospheric ion composition, Atmos. Meas. Tech., 3, 1039–1053, doi:10.5194/amt-3-1039-2010, 2010.

Kangasluoma, J., Junninen, H., Lehtipalo, K., Mikkilä, J., Vanhanen, J., Attoui, M., Sipilä, M., Worsnop, D., Kulmala, M., and Petäjä, T.: Remarks on Ion Generation for CPC Detection Efficiency Studies in Sub-3-nm Size Range, Aerosol Sci. Tech., 47, 556–563, doi:10.1080/02786826.2013.773393, 2013.

Kim, C. S., Okuyama, K., and de la Mora, J. F.: Performance evaluation of an improved particle size magnifier (PSM) for single nanoparticle detection, Aerosol Sci. Tech., 37, 791–803, 2003.

Kirkby, J., Curtius, J., Almeida, J., Dunne, E., Duplissy, J., Ehrhart, S., Franchin, A., Gagné, S., Ickes, L., Kürten, A., Kupc, A., Metzger, A., Riccobono, F., Rondo, L., Schobesberger, S., Tsagkogeorgas, G., Wimmer, D., Amorim, A., Bianchi, F., Breitenlechner, M., David, A., Dommen, J., Downard, A., Ehn, M., Flagan, R. C., Haider, S., Hansel, A., Hauser, D., Jud, W., Junninen, H., Kreissl, F., Kvashin, A., Laaksonen, A., Lehtipalo, K., Lima, J., Lovejoy, E. R., Makhmutov, V., Mathot, S., Mikkilä, J., Minginette, P., Mogo, S., Nieminen, T., Onnela, A., Pereira, P., Petäjä, T., Schnitzhofer, R., Seinfeld, J. H., Sipilä, M., Stozhkov, Y., Stratmann, F., Tomé, A., Vanhanen, J., Viisanen, Y., Vrtala, A., Wagner, P. E., Walther, H., Weingartner, E., Wex, H., Winkler, P. M., Carslaw, K. S., Worsnop, D. R., Baltensperger, U., and Kulmala, M.: Role of sulphuric acid, ammonia and galactic cosmic rays in atmospheric aerosol nucleation, Nature, 476, 429–433, doi:10.1038/nature10343, 2011.

Kontkanen, J., Lehtinen, K. E. J., Nieminen, T., Manninen, H. E., Lehtipalo, K., Kerminen, V.-M., and Kulmala, M.: Estimating the contribution of ion-ion recombination to sub-2 nm cluster concentrations from atmospheric measurements, Atmos. Chem. Phys., 13, 11391–11401, doi:10.5194/acp-13-11391-2013, 2013.

Kuang, C., Chen, M., McMurry, P. H., and Wang, J.: Modification of Laminar Flow Ultrafine Condensation Particle Counters for the Enhanced Detection of 1 nm Condensation Nuclei, Aerosol Sci. Tech., 46, 309–315, 2012a.

Kuang, C., Chen, M., Zhao, J., Smith, J., McMurry, P. H., and Wang, J.: Size and time-resolved growth rate measurements of 1 to 5 nm freshly formed atmospheric nuclei, Atmos. Chem. Phys., 12, 3573–3589, doi:10.5194/acp-12-3573-2012, 2012b.

Kulmala, M., Vehkamäki, H., Petäjä, T., Dal Maso, M., Lauri, A., Kerminen, V.-M., Birmili, W., and McMurry, P. H.: Formation and growth rates of ultrafine atmospheric particles: a review of observations, J. Aerosol Sci., 35, 143–176, 2004.

Kulmala, M., Riipinen, I., Sipilä, M., Manninen, H. E., Petäjä, T., Junninen, H., Maso, M. D., Mordas, G., Mirme, A., Vana, M., Hirsikko, A., Laakso, L., Harrison, R. M., Hanson, I., Leung, C., Lehtinen, K. E. J., and Kerminen, V.-M.: Toward Direct Measurement of Atmospheric Nucleation, Science, 318, 89–92, doi:10.1126/science.1144124, 2007.

Kulmala, M., Kontkanen, J., Junninen, H., Lehtipalo, K., Manninen, H. E., Nieminen, T., Petäjä, T., Sipilä, M., Schobesberger, S., Rantala, P., Franchin, A., Jokinen, T., Järvinen, E., Äijälä, M., Kangasluoma, J., Hakala, J., Aalto, P. P., Paasonen, P., Mikkilä, J., Vanhanen, J., Aalto, J., Hakola, H., Makkonen, U., Ruuskanen, T., Mauldin, R. L., Duplissy, J., Vehkamäki, H., Bäck, J., Kortelainen, A., Riipinen, I., Kurtén, T., Johnston, M. V., Smith, J. N., Ehn, M., Mentel, T. F., Lehtinen, K. E. J., Laaksonen, A., Kerminen, V.-M., and Worsnop, D. R.: Direct Observations of Atmospheric Aerosol Nucleation, Science, 339, 943–946, doi:10.1126/science.1227385, 2013.

Lehtipalo, K., Sipilä, M., Riipinen, I., Nieminen, T., and Kulmala, M.: Analysis of atmospheric neutral and charged molecular clusters in boreal forest using pulse-height CPC, Atmos. Chem. Phys., 9, 4177–4184, doi:10.5194/acp-9-4177-2009, 2009.

Lehtipalo, K., Kulmala, M., Sipilä, M., Petäjä, T., Vana, M., Ceburnis, D., Dupuy, R., and O'Dowd, C.: Nanoparticles in boreal forest and coastal environment: a comparison of observations and implications of the nucleation mechanism, Atmos. Chem. Phys., 10, 7009–7016, doi:10.5194/acp-10-7009-2010, 2010.

Lihavainen, H., Komppula, M., Kerminen, V.-M., Järvinen, H., Viisanen, Y., Lehtinen, K., Vana, M., and Kulmala, M.: Size distributions of atmospheric ions inside clouds and in cloud-free air at a remote continental site, Boreal Environ. Res., 12, 337–344, 2007.

Makkonen, R., Asmi, A., Kerminen, V.-M., Boy, M., Arneth, A., Hari, P., and Kulmala, M.: Air pollution control and decreasing new particle formation lead to strong climate warming, Atmos. Chem. Phys., 12, 1515–1524, doi:10.5194/acp-12-1515-2012, 2012.

Manninen, H. E., Petäjä, T., Asmi, E., Riipinen, I., Nieminen, T., Mikkilä, J., Horrak, U., Mirme, A., Mirme, S., and Laakso, L.: Long-term field measurements of charged and neutral clusters using Neutral cluster and Air Ion Spectrometer (NAIS), Boreal Environ. Res, 14, 591–605, 2009.

Manninen, H. E., Nieminen, T., Asmi, E., Gagné, S., Häkkinen, S., Lehtipalo, K., Aalto, P., Vana, M., Mirme, A., Mirme, S., Hõrrak, U., Plass-Dülmer, C., Stange, G., Kiss, G., Hoffer, A., Töro", N., Moerman, M., Henzing, B., de Leeuw, G., Brinkenberg, M., Kouvarakis, G. N., Bougiatioti, A., Mihalopoulos, N., O'Dowd, C., Ceburnis, D., Arneth, A., Svenningsson, B., Swietlicki, E., Tarozzi, L., Decesari, S., Facchini, M. C., Birmili, W., Sonntag, A., Wiedensohler, A., Boulon, J., Sellegri, K., Laj, P., Gysel, M., Bukowiecki, N., Weingartner, E., Wehrle, G., Laaksonen, A., Hamed, A., Joutsensaari, J., Petäjä, T., Kerminen, V.-M., and Kulmala, M.: EUCAARI ion spectrometer measurements at 12 European sites – analysis of new particle formation events, Atmos. Chem. Phys., 10, 7907–7927, doi:10.5194/acp-10-7907-2010, 2010.

Manninen, H. E., Franchin, A., Schobesberger, S., Hirsikko, A., Hakala, J., Skromulis, A., Kangasluoma, J., Ehn, M., Junninen, H., Mirme, A., Mirme, S., Sipilä, M., Petäjä, T., Worsnop, D. R., and Kulmala, M.: Characterisation of corona-generated ions used in a Neutral cluster and Air Ion Spectrometer (NAIS), Atmos. Meas. Tech., 4, 2767–2776, doi:10.5194/amt-4-2767-2011, 2011.

Merikanto, J., Spracklen, D. V., Mann, G. W., Pickering, S. J., and Carslaw, K. S.: Impact of nucleation on global CCN, Atmos. Chem. Phys., 9, 8601–8616, doi:10.5194/acp-9-8601-2009, 2009.

Metzger, A., Verheggen, B., Dommen, J., Duplissy, J., Prevot, A. S. H., Weingartner, E., Riipinen, I., Kulmala, M., Spracklen, D. V., Carslaw, K. S., and Baltensperger, U.: Evidence for the role of organics in aerosol particle formation under atmospheric conditions, P. Natl. Acad. Sci. USA, 107, 6646–6651, doi:10.1073/pnas.0911330107, 2010.

Mikkonen, S., Romakkaniemi, S., Smith, J. N., Korhonen, H., Petäjä, T., Plass-Duelmer, C., Boy, M., McMurry, P. H., Lehtinen, K. E. J., Joutsensaari, J., Hamed, A., Mauldin III, R. L., Birmili, W., Spindler, G., Arnold, F., Kulmala, M., and Laaksonen, A.: A statistical proxy for sulphuric acid concentration, Atmos. Chem. Phys., 11, 11319–11334, doi:10.5194/acp-11-11319-2011, 2011.

Mirme, A., Tamm, E., Mordas, G., Vana, M., Uin, J., Mirme, S., Bernotas, T., Laakso, L., Hirsikko, A., and Kulmala, M.: A wide-range multi-channel Air Ion Spectrometer, Boreal Environ. Res., 12, 247–264, 2007.

Mirme, S. and Mirme, A.: The mathematical principles and design of the NAIS – a spectrometer for the measurement of cluster ion

and nanometer aerosol size distributions, Atmos. Meas. Tech., 6, 1061–1071, doi:10.5194/amt-6-1061-2013, 2013.

Mirme, S., Mirme, A., Minikin, A., Petzold, A., Hõrrak, U., Kerminen, V. -M., and Kulmala, M.: Atmospheric sub-3 nm particles at high altitudes, Atmos. Chem. Phys., 10, 437–451, doi:10.5194/acp-10-437-2010, 2010.

Neitola, K., Asmi, E., Komppula, M., Hyvärinen, A.-P., Raatikainen, T., Panwar, T. S., Sharma, V. P., and Lihavainen, H.: New particle formation infrequently observed in Himalayan foothills – why?, Atmos. Chem. Phys., 11, 8447–8458, doi:10.5194/acp-11-8447-2011, 2011.

Paasonen, P., Nieminen, T., Asmi, E., Manninen, H. E., Petäjä, T., Plass-Dülmer, C., Flentje, H., Birmili, W., Wiedensohler, A., Hõrrak, U., Metzger, A., Hamed, A., Laaksonen, A., Facchini, M. C., Kerminen, V.-M., and Kulmala, M.: On the roles of sulphuric acid and low-volatility organic vapours in the initial steps of atmospheric new particle formation, Atmos. Chem. Phys., 10, 11223–11242, doi:10.5194/acp-10-11223-2010, 2010.

Petäjä, T., Mauldin, III, R. L., Kosciuch, E., McGrath, J., Nieminen, T., Paasonen, P., Boy, M., Adamov, A., Kotiaho, T., and Kulmala, M.: Sulfuric acid and OH concentrations in a boreal forest site, Atmos. Chem. Phys., 9, 7435–7448, doi:10.5194/acp-9-7435-2009, 2009.

Rose, C., Boulon, J., Hervo, M., Holmgren, H., Asmi, E., Ramonet, M., Laj, P., and Sellegri, K.: Long-term observations of cluster ion concentration, sources and sinks in clear sky conditions at the high-altitude site of the Puy de Dôme, France, Atmos. Chem. Phys., 13, 11573–11594, doi:10.5194/acp-13-11573-2013, 2013.

Sihto, S.-L., Kulmala, M., Kerminen, V.-M., Dal Maso, M., Petäjä, T., Riipinen, I., Korhonen, H., Arnold, F., Janson, R., Boy, M., Laaksonen, A., and Lehtinen, K. E. J.: Atmospheric sulphuric acid and aerosol formation: implications from atmospheric measurements for nucleation and early growth mechanisms, Atmos. Chem. Phys., 6, 4079–4091, doi:10.5194/acp-6-4079-2006, 2006.

Spracklen, D. V., Carslaw, K. S., Kulmala, M., Kerminen, V.-M., Sihto, S.-L., Riipinen, I., Merikanto, J., Mann, G. W., Chipperfield, M. P., and Wiedensohler, A.: Contribution of particle formation to global cloud condensation nuclei concentrations, Geophys. Res. Lett., 35, L06808, doi:10.1029/2007GL033038, 2008.

Tammet, H. and Kulmala, M.: Simulation tool for atmospheric aerosol nucleation bursts, J. Aerosol Sci., 36, 173–196, doi:10.1016/j.jaerosci.2004.08.004, 2005.

Vanhanen, J., Mikkilä, J., Lehtipalo, K., Sipilä, M., Manninen, H. E., Siivola, E., Petäjä, T., and Kulmala, M.: Particle Size Magnifier for Nano-CN Detection, Aerosol Sci. Tech., 45, 533–542, doi:10.1080/02786826.2010.547889, 2011.

Venzac, H., Sellegri, K., and Laj, P.: Nucleation events detected at the high altitude site of the Puy de Dôme Research Station, France, Boreal Environ. Res., 12, 345–359, 2007.

Venzac, H., Sellegri, K., Laj, P., Villani, P., Bonasoni, P., Marinoni, A., Cristofanelli, P., Calzolari, F., Fuzzi, S., and Decesari, S.: High frequency new particle formation in the Himalayas, P. Natl. Acad. Sci., 105, 15666–15671, 2008.

Venzac, H., Sellegri, K., Villani, P., Picard, D., and Laj, P.: Seasonal variation of aerosol size distributions in the free troposphere and residual layer at the puy de Dôme station, France, Atmos. Chem. Phys., 9, 1465–1478, doi:10.5194/acp-9-1465-2009, 2009.

Wang, J. and Wexler, A. S.: Adsorption of organic molecules may explain growth of newly nucleated clusters and new particle formation, Geophys. Res. Lett., 40, 2834–2838, doi:10.1002/grl.50455, 2013.

Wimmer, D., Lehtipalo, K., Franchin, A., Kangasluoma, J., Kreissl, F., Kürten, A., Kupc, A., Metzger, A., Mikkilä, J., Petäjä, T., Riccobono, F., Vanhanen, J., Kulmala, M., and Curtius, J.: Performance of diethylene glycol-based particle counters in the sub-3 nm size range, Atmos. Meas. Tech., 6, 1793–1804, doi:10.5194/amt-6-1793-2013, 2013.

Young, L.-H., Benson, D. R., Montanaro, W. M., Lee, S.-H., Pan, L. L., Rogers, D. C., Jensen, J., Stith, J. L., Davis, C. A., Campos, T. L., Bowman, K. P., Cooper, W. A., and Lait, L. R.: Enhanced new particle formation observed in the northern midlatitude tropopause region, J. Geophys. Res., 112, D10218, doi:10.1029/2006JD008109, 2007.